A Comparative Study of Probabilistic Models for Second-Order Hydrodynamic Responses of Offshore Platforms

Dong-Hyun Lim, *Yonghwan Kim

Department of Naval Architecture and Ocean Engineering, Seoul National University, Seoul, Korea
*yhwankim@snu.ac.kr

1 INTRODUCTION

Nonlinear hydrodynamic responses generally exhibit non-normal statistical behaviors, which complicates the prediction of response statistics. However, in many cases, a nonlinear hydrodynamic quantity can be represented in a two-term Volterra series if the dynamic problem is properly simplified. In this case, some analytic techniques can be applied to estimate the probability distribution of the nonlinear response. Representative examples are the sum-frequency vertical resonant vibration observed in tension-leg platforms (TLPs), and the horizontal slow-drift motion of moored floaters.

In this study, the Hermite-moment method by Winterstein (1988) is compared to the analytic formulation by Kac and Siegert (1947). Also, the probability distribution of response peaks for the two-term Volterra series with general bandwidth is derived. Aforementioned two examples of the second-order hydrodynamic responses are considered: the high-frequency springing motion and the slow-drift motion of a TLP.

2 MATHEHMATICAL FORMULATION

A second-order hydrodynamic response $Y(t)$ to a unidirectional random wave $X(t)$ can be represented in a two-term Volterra series with corresponding frequency-domain transfer functions. In a discretized form, $Y(t)$ is expressed as:

$$Y(t) = \mathrm{Re}\left[\sum_{j=1}^{\infty} A_j H_1(\omega_j) e^{i\omega_j t} + \sum_{j=1}^{\infty}\sum_{k=1}^{\infty} A_j A_k H_2(\omega_j, \omega_k) e^{i(\omega_j+\omega_k)t} + \sum_{j=1}^{\infty}\sum_{k=1}^{\infty} A_j A_k^* H_2(\omega_j, -\omega_k) e^{i(\omega_j-\omega_k)t} \right] \tag{1}$$

where A_j and ω_j are the complex amplitude and the frequency of j-th discretized wave component, and $H_1(\omega_j)$ and $H_2(\omega_j, \omega_k)$ are the LTF (linear transfer function) and the QTF (quadratic transfer function), respectively.

As shown by Kac and Siegert (1947), $Y(t)$ can be expanded with independent standardized Gaussian variates $W_j(t)$ as follows:

$$Y(t) = \sum_{j=1}^{N} \left[c_j W_j(t) + \lambda_j \left\{ W_j(t) \right\}^2 \right], \quad c_j = \left| \int_{-\infty}^{\infty} H_1(\omega) \sqrt{S_X(\omega)} \psi_j^*(\omega) d\omega \right| \tag{2}$$

In the equation above, $S_X(\omega)$ is the one-sided power spectrum of $X(t)$, and λ_j and ψ_j are the eigenvalue and the eigenvector of the following integral equation:

$$\int_{-\infty}^{\infty} \sqrt{S_X(\omega_1) S_X(\omega_2)} H_2(\omega_1, -\omega_2) \psi_j(\omega_2) d\omega_2 = \lambda_j \psi_j(\omega_1) \tag{3}$$

The characteristic function and the PDF (probability density function) of $Y(t)$ are then given by:

$$F_Y(\theta) = \int_{-\infty}^{\infty} p_Y(y) e^{i\theta y} dY = \prod_{j=1}^{\infty} \int_{-\infty}^{\infty} \frac{1}{\sqrt{2\pi}} e^{-\frac{1}{2}W^2} \cdot \left[e^{i\theta\left(c_j W + \lambda_j W^2\right)} \right] dW = \left[\prod_{j=1}^{\infty} \left(1 - 2i\lambda_j\theta\right)^{-1/2} \right] e^{-\sum_{j=1}^{\infty} \frac{c_j^2\theta^2}{2(1-2i\lambda_j\theta)}} \tag{4}$$

$$p_Y(y) = \frac{1}{2\pi} \int_{-\infty}^{\infty} F_Y(\theta) e^{-iy\theta} d\theta \tag{5}$$

Meanwhile, in the Hermite-moment method, $Y(t)$ is transformed to a standard normal process U(t) by following Hermite-polynomial expansion:

$$Y = m_Y + \kappa\sigma_Y \left[U + \sum_{n=3}^{4} \hat{h}_n He_{n-1}(U) \right] \tag{6}$$

where m_Y and σ_Y are the mean and the standard deviation of $Y(t)$, and He_n is the nth order Hermite polynomial. The coefficients κ, $\hat{h}_3$ and $\hat{h}_4$ are determined by matching the statistical moments of $Y(t)$ up to

fourth order. Detailed equations and the approximate solutions of those coefficients can be found in Yang et al. (2013).

For the two-term Volterra series $Y(t)$, the statistical moments used in applying the Hermite-moment method can also be analytically computed with aforementioned eigenvalues and eigenvectors. The nth cumulant k_n of $Y(t)$ is given by (Langley, 1987):

$$k_n = \sum_{j=1}^{N} \frac{1}{2(2\lambda_j)^n} \left\{ (n-1)! + \left(\frac{c_j}{2\lambda_j} \right)^2 n!(1-\delta_{n1}) \right\} \tag{7}$$

where δ_{ij} indicates the Dirac delta function. Then, the nth moment can be estimated by the relation of moments and cumulants.

The probability distribution of peaks of $Y(t)$ can be derived from that of the standard normal process $U(t)$. The PDF of peaks for $U(t)$ is given by:

$$\hat{p}_U(u) = \frac{1}{\sqrt{2\pi}} \left[\varepsilon e^{-\frac{u^2}{2\varepsilon^2}} + \sqrt{1-\varepsilon^2}\, u e^{-\frac{u^2}{2}} \int_{-\infty}^{\frac{u\sqrt{1-\varepsilon^2}}{\varepsilon}} e^{-\frac{1}{2}s^2} ds \right], \quad \varepsilon = \sqrt{1 - \frac{m_2^{\,2}}{m_0 m_4}} \tag{8}$$

where m_n is the nth spectral moment of $U(t)$. To estimate the bandwidth parameter ε, the second and fourth spectral moments of $U(t)$ are required. These can be derived from the following two equations relating the spectral density of $Y(t)$ and $U(t)$:

$$S_Y(\omega) = |H_1(\omega)|^2 S_X(\omega) + 8\int_0^{\infty} |H_2(\omega-\mu,\mu)|^2 S_X(|\omega-\mu|) S_X(|\mu|)\, d\mu \tag{9}$$

$$S_Y(\omega) = (\kappa\sigma_Y)^2 \left\{ S_U(\omega) + \sum_{n=3}^{N} (n-1)!\, \hat{h}_n^2 \left[S_U(\omega) \right]_{n-1} \right\} \tag{10}$$

where $S_Y(\omega)$ and $S_U(\omega)$ are the spectral density of $Y(t)$ and $U(t)$, respectively, and $[S_U(\omega)]_n$ in Eq. 10 indicates the n-fold convolution of $S_U(\omega)$. The equations for the first four spectral moments of $U(t)$ are then derived as:

$$\begin{aligned}
m_{Y,1} &= (\kappa\sigma_Y)^2 \left[m_1 + 2\hat{h}_3^{\,2} (2m_1) + 6\hat{h}_4^{\,2} (3m_1) \right] \\
m_{Y,2} &= (\kappa\sigma_Y)^2 \left[m_2 + 2\hat{h}_3^{\,2} (2m_2 + 2m_1^{\,2}) + 6\hat{h}_4^{\,2} (3m_2 + 6m_1^{\,2}) \right] \\
m_{Y,3} &= (\kappa\sigma_Y)^2 \left[m_3 + 2\hat{h}_3^{\,2} (2m_3 + 6m_2 m_1) + 6\hat{h}_4^{\,2} (3m_3 + 18m_2 m_1 + 6m_1^{\,3}) \right] \\
m_{Y,4} &= (\kappa\sigma_Y)^2 \left[m_4 + 2\hat{h}_3^{\,2} (2m_4 + 8m_3 m_1 + 6m_2^{\,2}) + 6\hat{h}_4^{\,2} (3m_4 + 24m_3 m_1 + 18m_2^{\,2} + 36m_2 m_1^{\,2}) \right]
\end{aligned} \tag{11}$$

where $m_{Y,n}$ indicates the nth spectral moment of $Y(t)$. Finally, the PDF of peaks of $Y(t)$ is given by:

$$\hat{p}_Y(y) = \hat{p}_U(u) \frac{du}{dy} \tag{12}$$

3 THE COMPUTATIONAL MODEL

The computational model used for the simulations is a TLP with 12 tendons and risers. Fig. 1 represents the configuration of the TLP and the coordinate system for describing the platform motion, and Figs. 2 and Fig. 3 represent the transfer functions for the heave and surge, respectively. The transfer functions were computed with a commercial software WADAM.

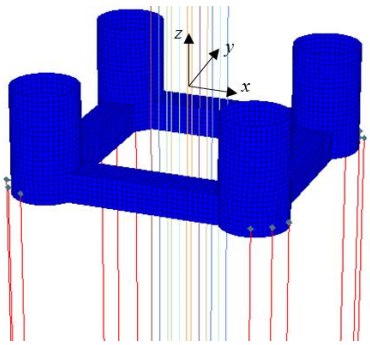

Fig. 1 The configuration of the TLP model

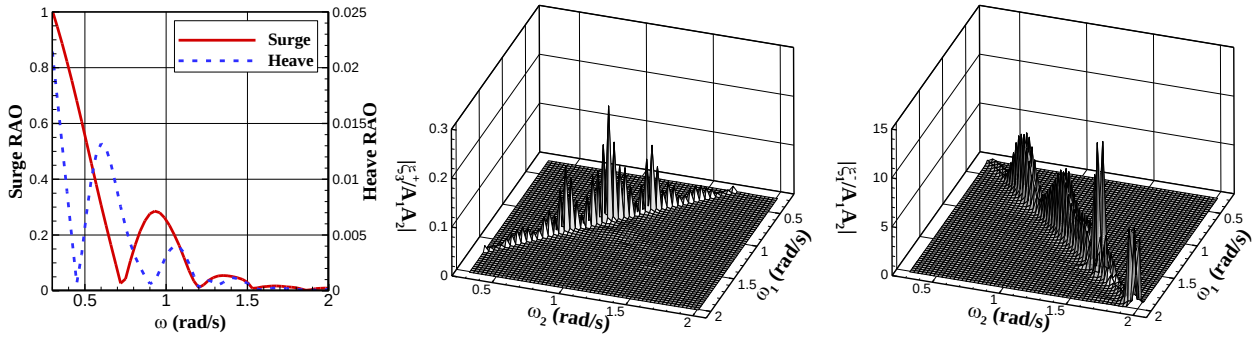

Fig. 2 Linear motion RAO (left), sum-frequency heave motion QTF (middle), and difference-frequency surge motion QTF (right)

4 THE COMPARISON TEST RESULTS

Two test conditions were constructed to investigate accuracy and applicability of the probabilistic models. In the first condition, termed Case 1, combined linear and sum-frequency heave motion is considered. The significant wave height H_S and the spectral peak period T_P were set to 6.0m and 12.0s, which induces linear and second-order motions comparable to each other. This results in a lower degree of kurtosis compared to the second-order resonance condition, but higher spectral bandwidth is induced. In the second condition, termed Case 2, combined linear and difference-frequency surge motion is investigated. An extreme wave condition with 12.0m of H_S and 16.0s of T_P was selected, which induces a strongly non-Gaussian and wide-banded surge motion. Details of each condition are summarized in Table 1.

Table 1 The simulation conditions and corresponding response statistics

	Mode	H_S (m)	T_P (s)	Skewness	Kurtosis	Bandwidth
Case 1	Heave	6.0	12.0	0.0	3.20	0.62
Case 2	Surge	12.0	16.0	0.44	3.68	0.93

Fig. 3 represents the PDFs of each motion in Case 1 and Case 2. A noticeable feature of the result is that the Hermite-moment method slightly overestimates the PDF around the tail in Case 1, while this tendency is not observed in Case 2 where the non-Gaussianity is stronger. This is quite a counter-intuitive feature considering that the Hermite-moment method is based on the transformation of $Y(t)$ to a standard normal process $U(t)$. Hence, it is inferred that accuracy of the Hermite-moment method does not necessarily decrease with increasing non-Gaussianity. However, the discrepancy is minor, and both of the probabilistic models exhibit great prediction of the sampling result.

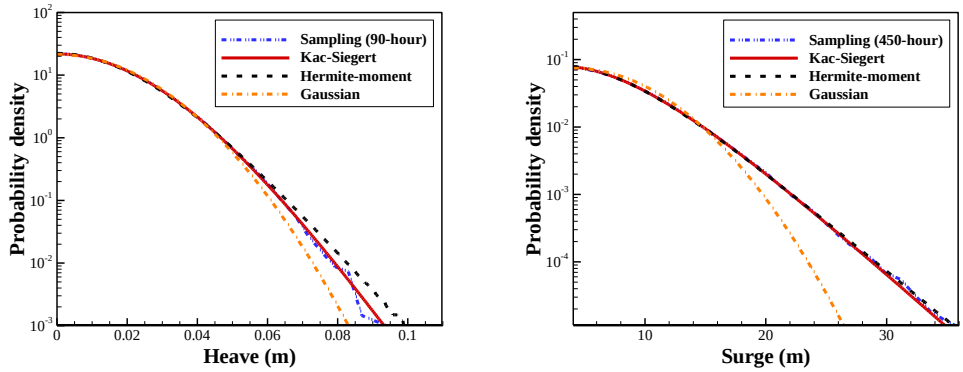

Fig. 3 The PDFs of the heave motion in Case 1 (left) and the surge motion in Case 2 (right)

Fig. 4 represents the exceedance probability distributions of response peaks in Case 1 and Case 2. From this figure, it is identified that the Hermite-moment model for general bandwidth (Eqs. 8~12) predicts the probability distribution of peaks with great accuracy. From negative peaks to the extreme ones, sampled peaks lie very close to the present prediction, whereas the result neglecting the bandwidth effect considerably overestimates the probability level. This discrepancy significantly affects the accuracy of fatigue damage estimation from the peak distribution. Fig. 5 represents the relative fatigue damage rate in the riser closest to the motion center estimated from the peak distribution with and without consideration of the bandwidth. Benasciutti (2004) was referred for the formulation of the rainflow fatigue damage from the peak distribution. It is observed that the present model predicts the fatigue damage rate with a very high degree of accuracy, while the prediction neglecting the bandwidth effect results in great overestimation.

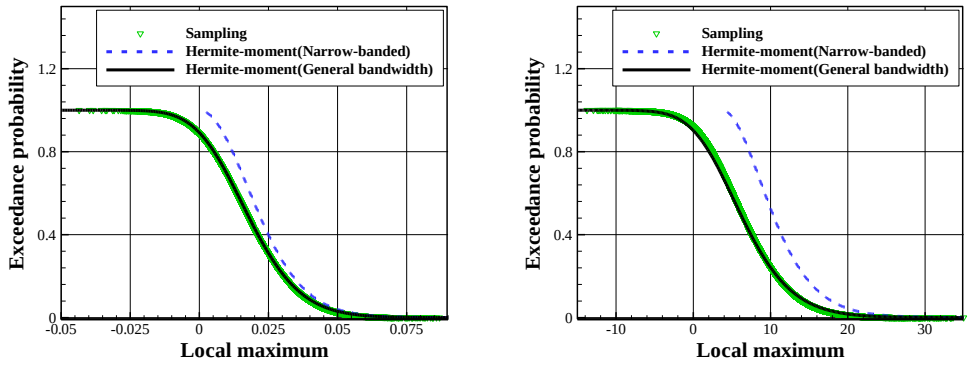

Fig. 4 The exceedance probability distributions of peaks in Case 1 (left) and Case 2 (right)

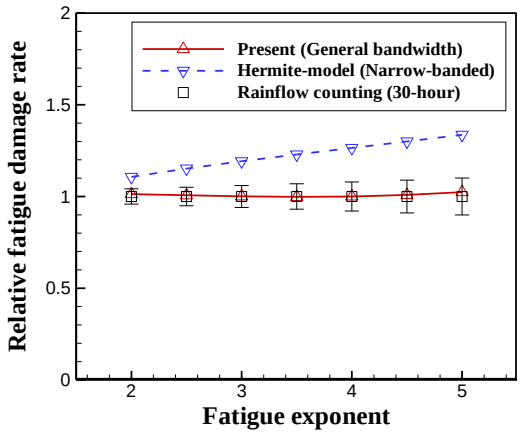

Fig. 5 The relative fatigue damage rate in the riser closest to the motion center

5 CONCLUSIONS

The Kac-Siegert method and the Hermite-moment method have been compared for predicting the

probabilistic behaviors of the second-order motions. The motion PDFs are predicted with high accuracy by both methods, but the Hermite-moment method may result in slight discrepancy when non-Gaussianity is mild, which is counter-intuitive. The probability distribution of response peaks considering the bandwidth effect has been derived and validated. The fatigue damage in the case of large bandwidth can be successfully estimated from the derived peak distribution.

ACKNOWLEDGEMENT

This study is supported by the Global Leading Technology Program of the Office of Strategic R&D Planning(OSP) which is funded by the Ministry of Trade, Industry and Energy, Republic of Korea (Project No: 10042556). Their supports are appreciated. Also the administrative support of AMEC and RIMSE at SNU should be acknowledged.

REFERENCES

Benasciutti, D., 2004. Fatigue Analysis of Random Loadings, Ph.D. Thesis, Univ. Ferrara.

Kac, M. & Siegert, A.J.F., 1947. An explicit representation of a stationary Gaussian process, Ann. Math. Stat., 18, 438–442.

Langley, R.S., 1987. A Statistical Analysis of Non-Linear Random Waves, Ocean Eng., 14(5), 389-407.

Winterstein, S.R., 1988. Nonlinear Vibration Models for Extremes and Fatigue, J. Eng. Mech., 114(10), 1772-1790.

Yang, L. et al., 2013. Probabilistic modeling of wind pressure on low-rise buildings, J. Wind Eng. Ind. Aero., 114, 18-26.

Lim, D.H., Kim, Y. 2016. Design Wave Method for the Extreme Horizontal Slow-drift Motion of Moored Floating Platforms, Applied Ocean Research (submitted for publication)

Lim, D.H., Kim, T.Y., Kim, Y. 2017. Stochastic Analysis of the Second-order Hydrodynamic Quantities for Offshore Structures (will appear)